1572–1582 *Nucleic Acids Research, 2020, Vol. 48, No. 3* *Published online 10 January 2020*
doi: 10.1093/nar/gkz1216

Crystal structure of human cytoplasmic tRNA^{His}-specific 5′-monomethylphosphate capping enzyme

Yining Liu, Anna Martinez, Seisuke Yamashita and Kozo Tomita *

Department of Computational Biology and Medical Sciences, Graduate School of Frontier Sciences, The University of Tokyo, Kashiwa, Chiba 277-8562, Japan

Received November 7, 2019; Revised December 15, 2019; Editorial Decision December 16, 2019; Accepted December 17, 2019

ABSTRACT

BCDIN3 domain containing RNA methyltransferase, BCDIN3D, monomethylates the 5′-monophosphate of cytoplasmic tRNA^{His} with a G_{-1}:A_{73} mispair at the top of an eight-nucleotide-long acceptor helix, using *S*-adenosyl-L-methionine (SAM) as a methyl group donor. In humans, BCDIN3D overexpression is associated with the tumorigenic phenotype and poor prognosis in breast cancer. Here, we present the crystal structure of human BCDIN3D complexed with *S*-adenosyl-L-homocysteine. BCDIN3D adopts a classical Rossmann-fold methyltransferase structure. A comparison of the structure with that of the closely related methylphosphate capping enzyme, MePCE, which monomethylates the 5′-γ-phosphate of 7SK RNA, revealed the important residues for monomethyl transfer from SAM onto the 5′-monophosphate of tRNA^{His} and for tRNA^{His} recognition by BCDIN3D. A structural model of tRNA^{His} docking onto BCDIN3D suggested the molecular mechanism underlying the different activities between BCDIN3D and MePCE. A loop in BCDIN3D is shorter, as compared to the corresponding region that forms an α-helix to recognize the 5′-end of RNA in MePCE, and the G_{-1}:A_{73} mispair in tRNA^{His} allows the N-terminal α-helix of BCDIN3D to wedge the G_{-1}:A_{73} mispair of tRNA^{His}. As a result, the 5′-monophosphate of G_{-1} of tRNA^{His} is deep in the catalytic pocket for 5′-phosphate methylation. Thus, BCDIN3D is a tRNA^{His}-specific 5′-monomethylphosphate capping enzyme that discriminates tRNA^{His} from other tRNA species, and the structural information presented in this study also provides the molecular basis for the development of drugs against breast cancers.

INTRODUCTION

BCDIN3D, bicoid interacting 3 domain containing RNA methyltransferase, is an evolutionarily conserved member of the Bin3 methyltransferase family and contains an *S*-adenosyl-L-methionine (SAM) binding domain (1,2). BCDIN3D is closely related to the methylphosphate capping enzyme (MePCE), also called BCDIN3 in humans, which catalyzes the monomethylation of the 5′-γ-phosphate of a small subset of noncoding RNAs using SAM as a methyl group donor (3–6). The primary target of MePCE is the ubiquitous 7SK RNA (5,6). 7SK RNA is a main component of a regulatory RNA–protein complex that downregulates the activity of an RNA polymerase II elongation factor, P-TEFb, consisting of a cyclin-dependent kinase CDK9 and cyclin T1/T2 (7,8). Monomethylation of the 5′-γ-phosphate of 7SK RNA protects 7SK from degradation and controls the activity of P-TEFb (5,6,9). In contrast, the biological function of BCDIN3D has remained enigmatic. Several reports have shown that BCDIN3D is often overexpressed in human breast cancer cells, and the elevated expression of BCDIN3D is associated with the tumorigenic phenotype and poor prognosis in breast cancer, particularly triple-negative breast cancers (1,10,11). Recently, studies in *Drosophila* revealed that BCDIN3D is involved in female fertility (12).

Until recently, the primary target of BCDIN3D had been unknown. Several years ago, it was reported that BCDIN3D catalyzes the dimethylation of the 5′-monophosphate of a specific group of precursor miRNAs, such as the tumor suppressor miR-145, and that the dimethylation of pre-miRNAs inhibits subsequent Dicer processing. As a result, the expression of the mature form of the tumor suppressor miRNA is suppressed (1). However, it was recently shown that BCDIN3D tightly interacts with cytoplasmic tRNA^{His} in HEK293 cells. An LC-nano ESI-MS analysis (13) of tRNA^{His} revealed that tRNA^{His} has a 5′-monomethylphosphate, as previously reported (14,15). It was also shown that BCDIN3D monomethylates the 5′-monophosphate of tRNA^{His} *in vitro*, and the

*To whom correspondence should be addressed. Tel: +81 (0)471363611; Fax: +81 (0)471363611; Email: kozo-tomita@edu.k.u-tokyo.ac.jp

BCDIN3D gene knockout in HEK293 cells results in the loss of the modification of $tRNA^{His}$ *in vivo*. At the same time, it was shown that BCDIN3D monomethylates $tRNA^{His}$ more efficiently than pre-miR-145 by over two orders of magnitude *in vitro*, and never dimethylates the 5′-monophosphate of $tRNA^{His}$, as revealed by an LC-nano ESI-MS analysis. BCDIN3D specifically recognizes the unique features observed only in $tRNA^{His}$, among the eukaryotic tRNA species. It recognizes the acceptor helix of $tRNA^{His}$ with a G_{-1}:A_{73} mispair at the top of the eight-nucleotide-long acceptor helix and the G_{-1} nucleobase. Therefore, it was concluded that BCDIN3D is a $tRNA^{His}$-specific monomethylphosphate capping enzyme (15,16).

Here, we present the crystal structure of human BCDIN3D (hBCDIN3D) complexed with *S*-adenosyl-L-homocysteine (SAH). The structural and biochemical studies of BCDIN3D, together with the structural comparison between BCDIN3D and MePCE, have revealed the mechanism of the specific methylation of the 5′-monophosphate of $tRNA^{His}$ by BCDIN3D, and confirmed that BCDIN3D is a $tRNA^{His}$-specific monomethylphosphate capping enzyme. The structural information presented in this study also provides the molecular basis for the development of drugs against breast cancers.

MATERIALS AND METHODS

Plasmid constructions

The DNA fragments encoding BCDIN3D proteins from various organisms were synthesized by Eurofins, Japan. The synthesized nucleotide sequences are shown in Supplementary Table S1. For overexpression, the BCDIN3D gene sequences were cloned between the NdeI and XhoI sites of the pET-15b vector (Merck Millipore, Japan). The mutations in the BCDIN3D gene were introduced by the inverse PCR method. The oligonucleotide sequences used for the plasmid constructions are listed in Supplementary Table S2.

Protein expression and purification

Escherichia coli BL21(DE3) cells (Novagen-Merck Millipore) were transformed with the plasmids and grown in LB medium containing 50 μg/ml ampicillin at 37°C, until A_{600} reached 0.8. The expression of BCDIN3D and its variants was induced by the addition of isopropyl-β-D-thiogalactopyranoside at a final concentration of 0.1 mM, and the culture was continued for 16 h at 20°C. The cells were harvested and sonicated, in buffer containing 20 mM Tris–HCl, pH 7.0, 500 mM NaCl, 10 mM β-mercaptoethanol, 5% (v/v) glycerol and 20 mM imidazole (buffer A), and centrifuged at 100 000 × *g* for 1 h at 4°C. The clear supernatant was applied to a Ni-NTA agarose column (Qiagen, Japan), and after the column was washed with buffer A, the proteins were eluted from the column with buffer containing 20 mM Tris–HCl, pH 7.0, 500 mM NaCl, 5% (v/v) glycerol, 250 mM imidazole and 10 mM β-mercaptoethanol. The proteins were further purified on a HiTrap Heparin column (GE Healthcare, Japan), and finally applied to a HiLoad 16/60 Superdex 200 column (GE Healthcare, Japan), equilibrated with buffer containing 20 mM Tris–HCl, pH 7.0, 200 mM NaCl and 10 mM β-mercaptoethanol. The purified proteins were concentrated, and stored at −80°C.

Crystallization and structural determination

The hBCDIN3D_t protein, the truncated form of hBCDIN3D, was adjusted to 2 mg/ml and supplemented with 1 mM SAH (Sigma) and 22.2 mM Tris–HCl, pH 8.0, for neutralization. A 0.3 μl portion of the protein solution was mixed with 0.2 μl of reservoir solution, containing 20% (w/v) PEG 3350 and 200 mM $CaCl_2$. The crystals were generated by the sitting drop vapor diffusion method at 20°C. To facilitate the crystallization, the drop was supplemented with 100 nl of crystal seed solution, prepared with Seed Bead (Hampton Research), in buffer containing 100 mM sodium cacodylate, pH 7.0, 25% (v/v) tacsimate, pH 7.0, and 1 mM spermine.

Data sets were collected at beamline 17A at the Photon Factory at KEK, Japan. The crystals were flash-cooled in a solution containing 15% (w/v) PEG 3350, 150 mM $CaCl_2$, 8.3% tacsimate, pH 7.0, 33 mM sodium cacodylate, pH 7.0, 0.33 mM spermine and 20% (v/v) ethylene glycol.

The data were indexed, integrated and scaled with XDS (17). The diffraction data were processed by the STARANISO server (http://staraniso.globalphasing.org/cgi-bin/staraniso.cgi) for anisotropy correction and truncation. The initial phase was determined by the molecular replacement method, using the Phaser program (18). As the search model, a homology model was prepared by the SWISS-MODEL server (19), based on the crystal structure of the human methylphosphate capping enzyme, MePCE (PDB ID: 5UNA). The structure was refined with phenix.refine (20), and manually modified with Coot (21).

In vitro methylation assay

The methylation assays were performed as described (15), with some modifications. For assays using [^{14}C]-SAM, reaction mixtures (20 μl) containing 50 mM Tris–HCl, pH 8.0, 50 mM NaCl, 5 mM $MgCl_2$, 2 mM DTT, 5% (v/v) glycerol, 1 μM RNA, 10 μM [^{14}C]-SAM (40 mCi/mmol, PerkinElmer, Japan) and 1 μM BCDIN3D from various organisms were incubated at 37°C. The RNAs were phenol–chloroform extracted, ethanol precipitated and separated by 10% (w/v) polyacrylamide gel electrophoresis under denaturing conditions. The gel was dried and exposed to an imaging plate, and the methylated RNAs were detected with a BAS-5000 imager (Fujifilm, Japan).

For assays using [^{3}H]-SAM, reaction mixtures (20 μl) containing 50 mM Tris–HCl, pH 8.0, 50 mM NaCl, 5 mM $MgCl_2$, 2 mM DTT, 5% (v/v) glycerol, 1 μM RNA, 10 μM [^{3}H]-SAM (55 mCi/mmol, PerkinElmer, Japan) and 0.1 μM BCDIN3D or its variants were incubated at 37°C. An aliquot (10 μM) was withdrawn at the indicated time from the reaction solution and spotted onto a Whatman 3MM filter (GE Healthcare, Japan). Under this condition, the reaction by wild-type BCDIN3D proceeds in a linear range until 10 min. After the filters were washed with 10%

(w/v) TCA, they were washed with ethanol and dried. The filters were suspended in Ultima Gold liquid scintillation cocktail (PerkinElmer, Japan), and the radioactivities on the filters were quantified with a liquid scintillation counter (Beckman Coulter).

Human $tRNA^{His}$ transcripts were synthesized by T7 RNA polymerase in the presence of excess GMP, and purified by 10% (w/v) polyacrylamide gel electrophoresis under denaturing conditions. To prepare the $tRNA^{His}$ transcript with a 5′-triphosphate, GMP was omitted from the reaction, and it was purified in the same manner.

tRNA docking model onto BCDIN3D

A model of $tRNA^{His}$ with G_{-1}:A_{73} mispair at the top of the acceptor helix onto BCDIN3D was manually built as follows using program Coot (21). The backbone of the modeled tRNA with G_{-1}:A_{73} mispair at the top of the eight-nucleotide-long acceptor helix of human $tRNA^{His}$ was derived from the crystal structure of initiator $tRNA_f^{Met}$ from *E. coli* (PDB ID: 3CW6) with C_1:A_{72} mispair at the top of the acceptor helix and flipped 5′-end nucleotide. First, the $tRNA_f^{Met}$ was manually superposed on the 5′-region of SL1p complexed with human MePCE (hMePCE), so that the 5′-α-phosphate of $tRNA_f^{Met}$ is placed in the catalytic site of BCDIN3D. Then, the 5′-end nucleotide C_1 of $tRNA_f^{Met}$ was replaced with G_{-1} and 3′-$A_{72}A_{73}C_{74}C_{75}A_{76}$ of $tRNA_f^{Met}$ was replaced with $A_{73}C_{74}C_{75}A_{76}$, and one base pair was inserted in the acceptor helix to generate the $tRNA^{His}$ model with eight-nucleotide-long acceptor stem. Finally, nucleotide sequence of the modeled acceptor helix was replaced with that of human $tRNA^{His}$.

RESULTS

Determination of the hBCDIN3D structure

Initial crystallization trials of full-length hBCDIN3D generated no diffractive crystals. Thus, we prepared the truncated form of hBCDIN3D, based on the sequence alignments with the BCDIN3D proteins from chicken, frog, zebrafish and fly, which were all capable of transferring the methyl group of SAM onto the human $tRNA^{His}$ transcript *in vitro* (Supplementary Figures S1 and S2). The N-terminal, internal and C-terminal putative flexible regions, which are less conserved among them (residues 1–13, 92–99 and 285–292, respectively), were removed from hBCDIN3D, yielding hBCDIN3D_t (residues 14–284_Δ92–99; Figure 1A). hBCDIN3D_t had around 25% methylation activity of the full-length hBCDIN3D for the human $tRNA^{His}$ transcript (Figure 1B). Finally, we obtained diffractive crystals of hBCDIN3D_t in the presence of SAH.

The crystal belongs to the space group $P2_1$, and contains four hBCDIN3D molecules in the asymmetric unit. The initial phase was determined by the molecular replacement method, using a homology model of hBCDIN3D based on the structure of the methyltransferase domain (MTD) of MePCE (PDB ID: 5UNA), as the search model. The structure was model-built and refined to an R factor of 21.2% (R_{free} = 27.0%) at 2.9 Å resolution (Supplementary Figure S3). The final model contains residues 29–91 and 100–264 of hBCDIN3D (Figure 1C). The details of the crystallographic data collection and refinement statistics are shown in Table 1.

Table 1. Data collection and refinement statistics

	hBCDIN3D_t
Data collection	
Space group	$P2_1$
Cell dimensions	
a, *b*, *c* (Å)	48.14, 140.34, 86.42
β (°)	105.44
Wavelength (Å)	0.98000
Resolution (Å)[a]	50–2.9 (3.03–2.92)
No. of measured reflections	218 829
No. of unique reflections	23 888
R_{sym}[a]	0.205 (2.190)
$I/\sigma I$[a]	8.3 (1.2)
$CC_{1/2}$[a]	0.996 (0.693)
Completeness (%)[a]	99.8 (99.3)
Redundancy[a]	9.2 (9.0)
Refinement	
Resolution (Å)	50–2.9
No. reflections	20 740
R_{work}/R_{free} (%)	21.19/27.03
No. atoms	
Protein	7482
Ligand	104
Water	7
B-factors (Å^2)	
Protein	46.56
Ligand	29.36
Water	29.20
Root-mean-square deviations (RMSDs)	
Bond lengths (Å)	0.005
Bond angles (°)	0.86

[a]Values in parentheses are for the highest-resolution shell.

Overall structure of hBCDIN3D and SAH recognition

hBCDIN3D consists of eight α-helices (α1–α6, α5′ and α6′) and seven β-strands (β1–β7) (Figure 1C and D). The numbering of the α-helices and β-strands in hBCDIN3D follows that of the closely related MePCE structure for comparison (22) (Figure 2A).

The core of hBCDIN3D adopts a classical α/β methyltransferase fold, or the so-called Rossmann fold, with the parallel β-sheet containing a topological switch in the center. It consists of seven β-strands (β1–β7) and six α-helices (α1–α6), and the β-strands form an extended β-sheet with the α-helices sandwiching both sides of the β-sheet (Figures 1C and D, and 2A). The core of the BCDIN3D structure is homologous to those of other methyltransferases in the same family, such as MePCE (22), METTL16 (23,24), NSUN6 (25), TRAM61A (26) and DNMT1 (27) (Supplementary Figures S4 and S5). Additional α-helices, α5′ and α6′, are inserted between β4 and α5, and between β5 and α6, respectively, in the BCDIN3D structure (Figures 1C and D, and 2A).

In the structure of hBCDIN3D bound with SAH (Figure 1C), SAH resides in the cleft formed at the topological switch in the center of the Rossmann fold, and exten-

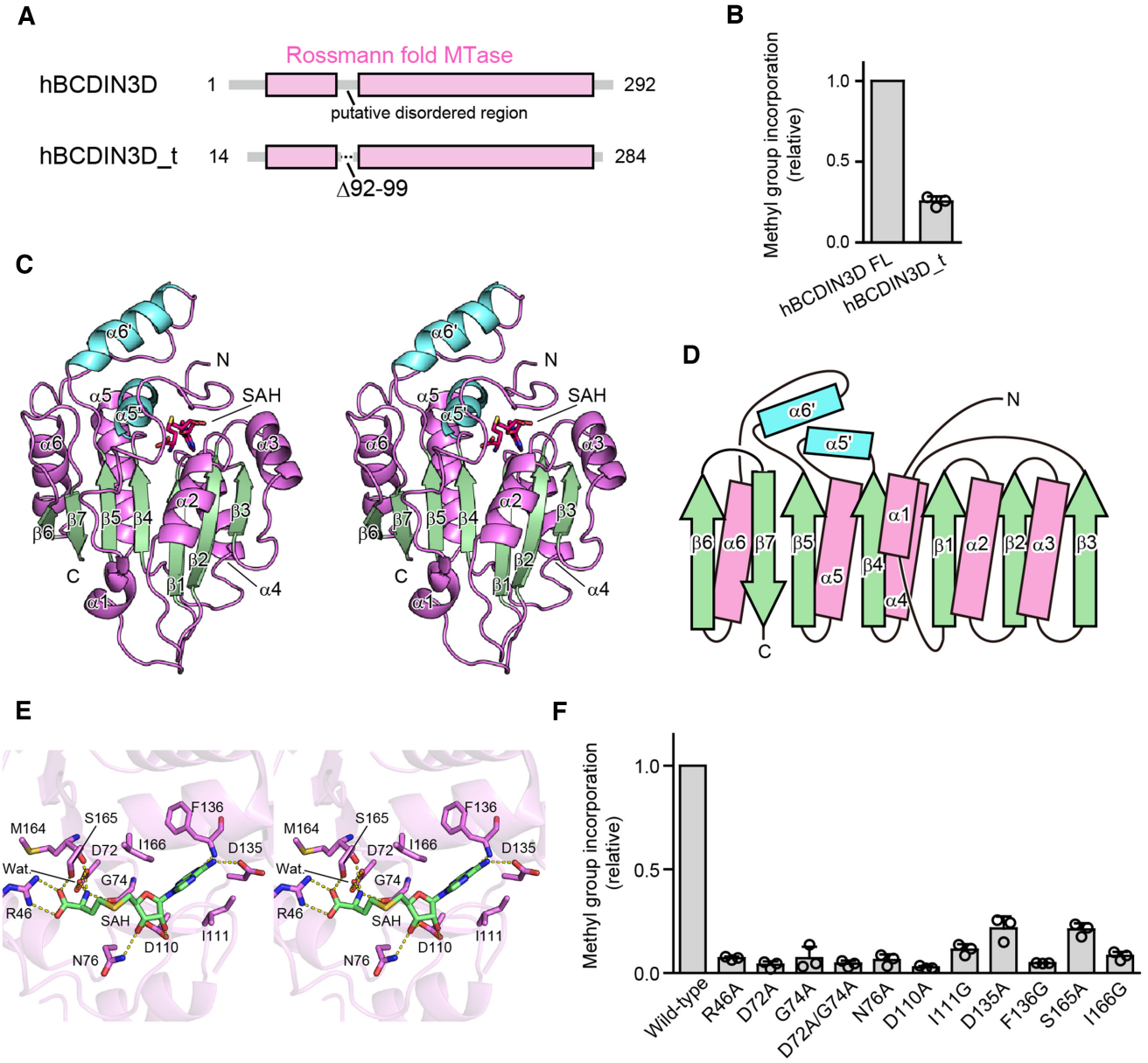

Figure 1. Overall structure of hBCDIN3D and SAH recognition. (**A**) Schematic diagrams of hBCDIN3D and its variant hBCDIN3D_t used for crystallization. (**B**) Relative methylation activity of hBCDIN3D_t (hBCDIN3D as 1.0) under standard conditions. The reaction mixtures were incubated at 37°C for 8 min. At this time point, the reaction by wild-type BCDIN3D proceeds in a linear range. Data are presented as mean ± standard deviation (SD) of three independent assays. (**C**) Stereo view of the ribbon model of hBCDIN3D, complexed with SAH. Residues 29–91 and 100–264 are modeled in the structure. SAH molecule is depicted by a red stick model. The α-helices and β-strands in the Rossmann fold are colored purple and green, respectively. Additional α-helices, α5′ and α6′, are colored cyan. (**D**) Topology diagram of hBCDIN3D. hBCDIN3D adopts the classical Rossmann fold. The colors are the same as in (C). (**E**) Stereo view of the SAH binding site of hBCDIN3D. SAH is depicted by a green stick model. (**F**) The activities of hBCDIN3D variants relative to the wild type (taken as 1.0) under the standard conditions. The reaction mixtures were incubated at 37°C for 1 h. Data are presented as mean ± SD of three independent assays.

sively interacts with hBCDIN3D through highly conserved residues (Figure 1E, Supplementary Figure S1). The N-terminal region of hBCDIN3D covers the SAH in the cleft, suggesting the enclosed catalytic site. R46 and S165 form hydrogen bonds with the SAH carboxylate group, and the main-chain carboxyl oxygens of G74 and M164 form hydrogen bonds with the SAH homocysteine amide group. D72 also forms a hydrogen bond with the homocysteine amide group, via a water molecule. I111 and I166 stack with the adenine base and sandwich it. D135 and the main-chain amide group of F136 form hydrogen bonds with the N6 and N1 atoms of the adenine base, respectively. The Nδ2 atom of D76 forms a hydrogen bond with the 3′-OH of the ribose, and D110 forms hydrogen bonds with the 2′-OH and 3′-OH of the ribose.

In vitro methylation reactions of the human $tRNA^{His}$ transcript using mutant hBCDIN3Ds (Figure 1F) showed that the R46A, D72A, G74A, D72A/G74A, D76A,

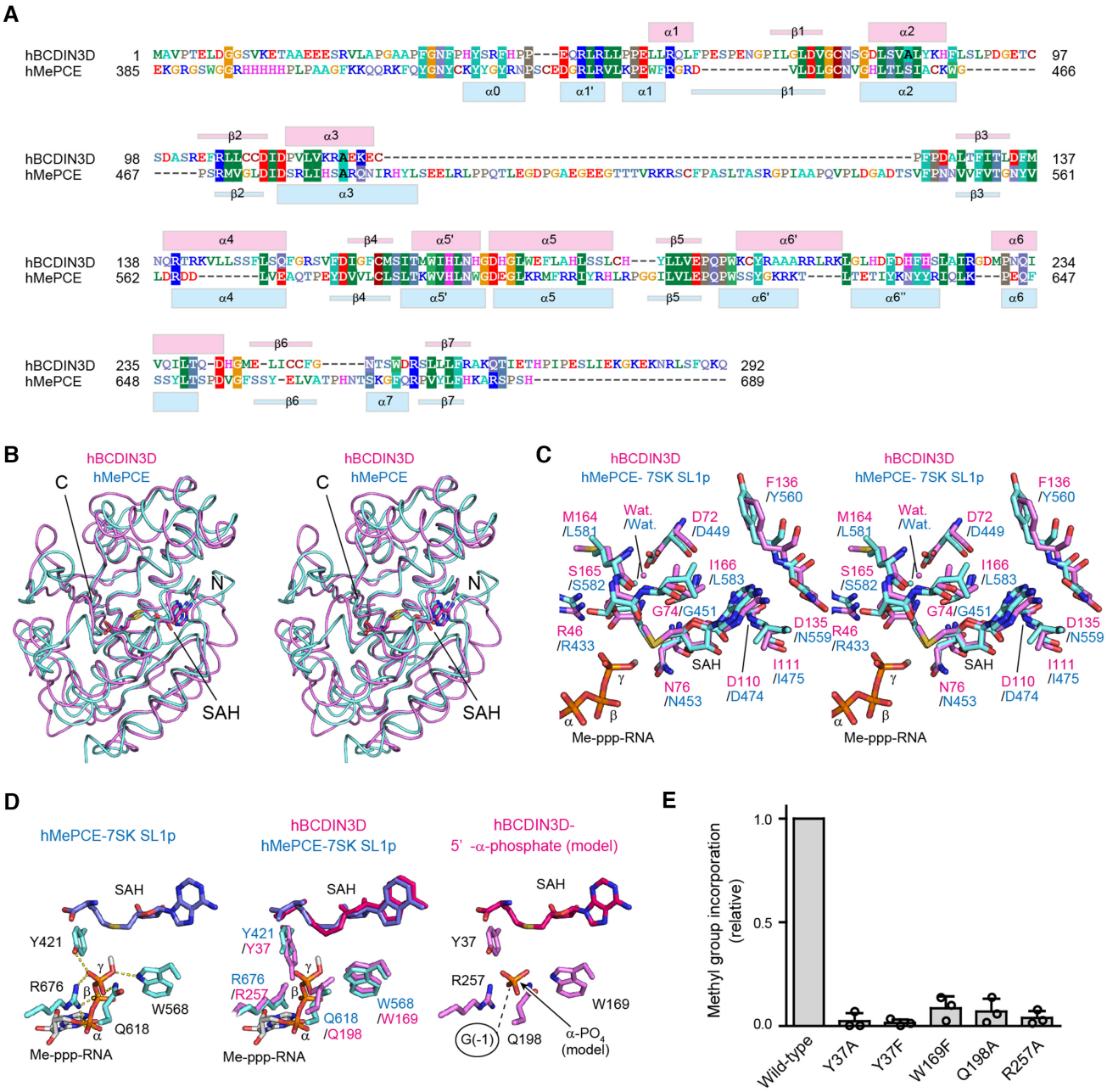

Figure 2. Comparison between hBCDIN3D and hMePCE. (**A**) Sequence alignment of hBCDIN3D and the MTD of hMePCE. The secondary structure elements of hBCDIN3D and hMePCE are indicated above and below the alignment, respectively. (**B**) Stereo view of the superimposed structures of hBCDIN3D (purple) and hMePCE (cyan). SAH molecules are depicted by stick models. (**C**) Superimposition of the structure of the SAH binding pocket of hBCDIN3D (purple) onto that of hMePCE (cyan) complexed with SAH and 7SK SL1p bearing a monomethyl-γ-phosphate 5′-cap (Me-ppp). The Me-ppp group at the 5′-G_1 of SL1p is shown as a stick model. (**D**) 5′-Phosphate recognition by hMePCE (left). Conserved residues for 5′-phosphate recognition by hBCDIN3D (purple) and hMePCE (cyan) (middle). Possible binding site of the 5′-α-phosphate of the G_{-1} of $tRNA^{His}$ in hBCDIN3D. The phosphate group is depicted by an orange stick model. (**E**) The activities of hBCDIN3D variants relative to the wild type (taken as 1.0) under the standard conditions. The reaction mixtures were incubated at 37°C for 1 h. Data are presented as mean ± SD of three independent assays.

D110A and F136G mutants abolished the enzymatic activity. The I111G, D135A, S165A and I166G mutants reduced the activity to extents of 10% or less than that of the wild type even at the reaction end points. Thus, these conserved residues are important for the SAM recognition and the methyltransferase activity of hBCDIN3D.

Mechanism of 5′-monophosphate recognition by hBCDIN3D

Quite recently, the crystal structures of the C-terminal MTD of the hMePCE, bound to SAH and RNAs, have been reported (22). hMePCE monomethylates the 5′-γ-phosphate of a small subset of noncoding RNAs, such as the 7SK and U6 snRNAs, using SAM as a methyl group donor (3–5).

The hBCDIN3D structure is quite homologous to that of the MTD of hMePCE, with 31% amino acid sequence identity and an RMSD of 2.1 Å for 181 structurally equivalent residues (calculated by the Dali server (28); RMSD calculated with the Cα atoms). The overall structures superimposed well on each other (Figure 2A and B).

The structure of the catalytic pocket of hBCDIN3D complexed with SAH was superimposed onto that of the MTD of hMePCE complexed with SAH and 7SK SL1p, a short RNA hairpin mimicking 7SK bearing a 5′-Me-ppp cap (Figure 2C). The hMePCE structure represents the termination stage of methylation. The SAH-interacting residues in hBCDIN3D described earlier (Figure 1E) superimposed well onto the corresponding residues in hMePCE (Figure 2C). Furthermore, the residues (Y421, R676, Q618 and W568; Figure 2D, left) interacting with the γ-phosphate oxygen of the 5′-G_1 of SL1p in the hMePCE structure also superimposed well onto the residues in the catalytic pocket of the hBCDIN3D structure (residues Y37, R257, Q198 and W169, respectively) (Figure 2D, middle). In hBCDIN3D, the OH group of Y37, the Nε atom of Q198, the Nε atom of W169 and R257 would form hydrogen bonds with the monophosphate oxygen at the 5′-end G_{-1} of $tRNA^{His}$ for methylation. In support of the formation of these hydrogen bonds, the Y37F, Y37A, W169F, Q198A and R257A mutants all abolished the enzymatic activity onto the $tRNA^{His}$ transcript (Figure 2E). At the reaction stage of the methylation of the 5′-phosphate of $tRNA^{His}$ by hBCDIN3D, the deprotonated and negatively charged α-phosphate oxygen under the neutral pH conditions would be positioned in the proximity of the SAM methyl group, and could nucleophilically attack the positively charged methyl sulfonium moiety of SAM for methylation, as proposed in the mechanism of the γ-phosphate methylation of 7SK RNA by hMePCE (22).

For the methylation of the $tRNA^{His}$ 5′-α-phosphate, the location of the 5′-nucleoside (G_{-1}) of $tRNA^{His}$ relative to the catalytic site in hBCDIN3D during the methyl transfer reaction should be closer to the catalytic site than the location of the 5′-nucleoside, G_1, of 7SK SL1p observed in the structure of hMePCE complexed with SL1p. The different activities between hBCDIN3D and hMePCE are described later.

A model of $tRNA^{His}$ docking onto hBCDIN3D

The electrostatic surface potential of hBCDIN3D shows a highly localized positively charged area, which is proximal to the catalytic SAM (SAH) binding pocket (Figure 3A). In particular, the positively charged residues are clustered on α6′ and are well conserved among the BCDIN3D proteins from various organisms (Supplementary Figure S1). The R257 residue in the loop between β6 and β7, and R118 in α3 are also proximal to the active pocket. As described earlier, R257 could interact with the α-phosphate oxygen of the 5′-end of $tRNA^{His}$ (Figure 2D, right). The recently reported crystal structure of the MTD of hMePCE, complexed with SAH and SL1p with a 5′-Me-ppp cap, showed a similar positively charged area, and the corresponding region in hMePCE, in particular α6′ and α3 (Figures 2A and 3B), participated in the recognition of the 5′ and 3′ parts of 7SK SL1p, respectively (22).

The K201A/R204A, R209A, R208A/R209A, R211A, R211A/K212A and R257A mutants of hBCDIN3D abolished the methylation activity with the $tRNA^{His}$ transcript *in vitro* (Figure 3C and D, Supplementary Figure S2B). The R201A, R204A, R208A and R212A mutants of hBCDIN3D also reduced the methylation activity, to extents of ∼10–20% of the wild-type activity *in vitro* (Figure 3D). The R118A mutation in α3 modestly reduced the activity, to ∼70% of the wild-type activity. Thus, these residues in hBCDIN3D would participate in the recognition of $tRNA^{His}$.

Based on the comparison of the structure of hBCDIN3D with that of hMePCE complexed with 7SK SL1p, and the superimposition of these two structures, a $tRNA^{His}$ docking model onto hBCDIN3D was built (Figure 4A and B). In the docking model, only the acceptor helix of $tRNA^{His}$ interacts with hBCDIN3D, and in particular, the basic α6′ helix interacts with the major groove of the acceptor helix (Figure 4C). The N-terminal region, which possibly forms an α-helix upon $tRNA^{His}$ binding, as described later, interacts with the 3′-single-stranded region and wedges the G_{-1}:A_{73} mispair at the top of the acceptor helix of $tRNA^{His}$. As a result, G_{-1} of $tRNA^{His}$ is relocated into the catalytic pocket for 5′-phosphate oxygen methylation, and the 3′-end is shifted toward α3 (Figure 4B and C). This model is consistent with the results showing that mutations of the basic amino acid residues in α6′ reduced the methylation activity onto $tRNA^{His}$ (Figure 3D). The impact of R118A in α3, which would interact with the 3′-single-stranded part of $tRNA^{His}$, is modest (Figure 3D, Supplementary Figure S2B), consistent with the previous data showing that the deletion of the 3′-CCA of $tRNA^{His}$ has minimal effects on the methylation by hBCDIN3D *in vitro* (15). Furthermore, mutations of the N-terminal region of BCDIN3D also reduced the methylation activity with $tRNA^{His}$ *in vitro*, suggesting the involvement of this N-terminal region in the methylation of the 5′-phosphate of $tRNA^{His}$ by hBCDIN3D, as described later.

Recognition of the top part of the $tRNA^{His}$ acceptor helix by hBCDIN3D

The amino acid sequences in the N-terminal region are conserved among the BCDIN3D proteins from various organisms, as well as among the MePCEs (Supplementary Figure S1, Figures 2A and 5A). In the structure of hMePCE complexed with 7SK SL1p, the corresponding N-terminal region forms an α-helix (α0, Figures 2A and 5B, left and middle), which is enriched with aromatic residues (Y421, Y422 and Y424) and hydrogen bonds with the 5′-triphosphate of G_1 of SL1p (Figure 5C, left). In particular, the OH group of Y421 forms a hydrogen bond with the 5′-γ-phosphate oxygen of SL1p, and the OH groups of Y418 and Y424 form hydrogen bonds with the 5′-β-phosphate oxygen of SL1p. The α0 helix of hMePCE interacts with the 3′-single-stranded regions of SL1p through hydrogen bonds and hydrophobic stacking interactions, as well as with SAH (Fig-

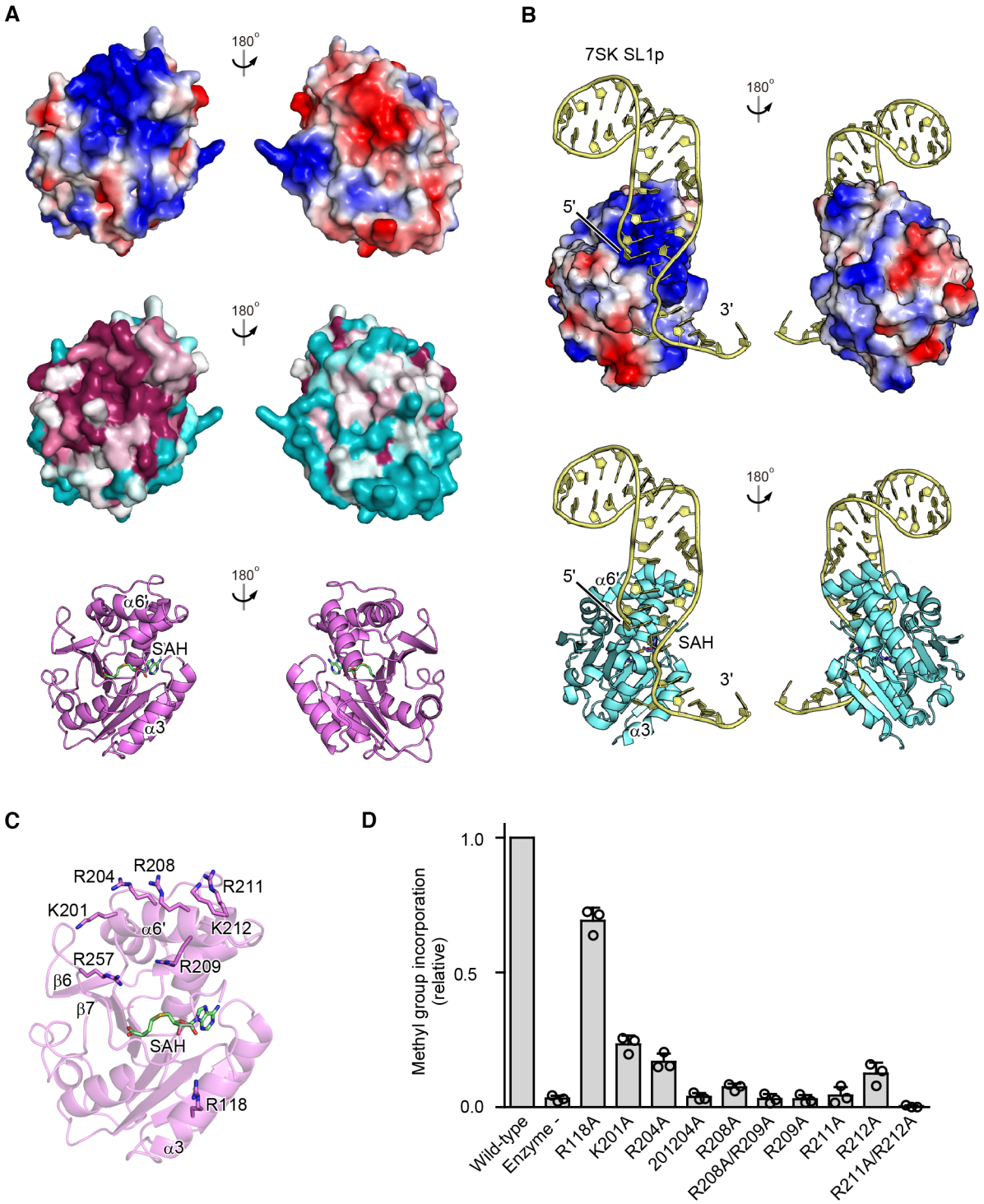

Figure 3. tRNA binding region in hBCDIN3D. (**A**) Electrostatic surface potential of hBCDIN3D (top). The positively and negatively charged regions are colored blue and red, respectively. Conservation analysis of hBCDIN3D (middle). Conserved and nonconserved residues are colored purple and cyan, respectively. The positively charged area is highly localized and conserved, and is proximal to the catalytic SAM binding pocket. (**B**) Electrostatic surface potential of the MTD of hMePCE complexed with 7SK SL1p (yellow) (22). The structure of hMePCE is viewed from the same direction as that of hBCDIN3D superimposed on hMePCE in (A). The positively and negatively charged regions are colored blue and red, respectively, and the distribution of the positively charged area is similar to that of hBCDIN3D. (**C**) Basic amino acid residues in hBCDIN3D that are possibly involved in the RNA recognition are depicted by sticks. (**D**) The activities of hBCDIN3D variants relative to the wild type (taken as 1.0) under the standard conditions. The reaction mixtures were incubated at 37°C for 8 min. At this time point, the reaction by wild-type BCDIN3D proceeds in a linear range (Supplementary Figure S2B). Data are presented as mean ± SD of three independent assays.

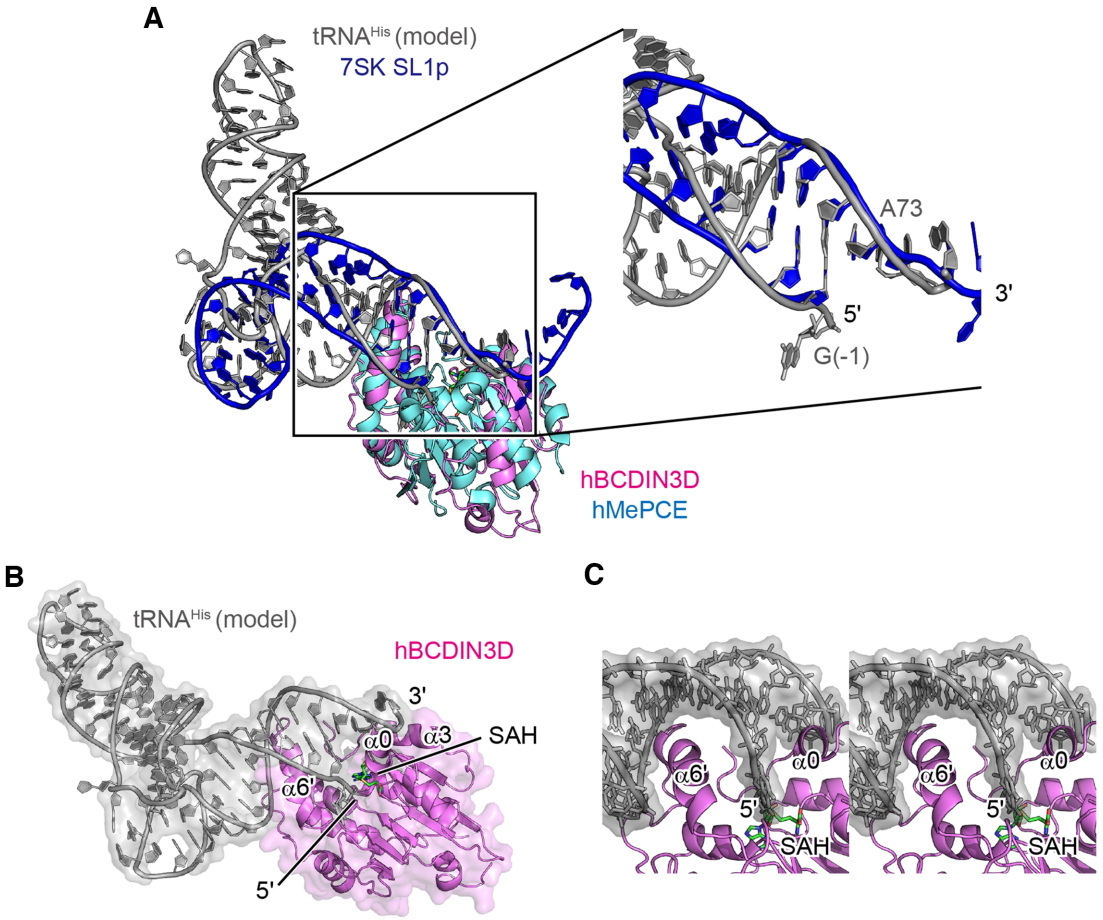

Figure 4. A model of tRNA docking onto hBCDIN3D. (**A**) Docking of tRNA^{His} onto hBCDIN3D. Superimposition of hBCDIN3D (purple) on the structure of the MTD of hMePCE (cyan) complexed with 7SK SL1p (blue). tRNA^{His} (gray) was modeled such that the acceptor helix of tRNA^{His} superimposed well onto the 5′-end and 3′-single-stranded region of SL1p. See 'Materials and Methods' section for details. (**B**) α6′ would interact with the major groove of the acceptor helix of tRNA^{His}, and α0 would wedge the G_{-1}:A_{73} mispair of tRNA^{His}. (**C**) A detailed stereo view of the interaction between the acceptor helix of tRNA^{His} and BCDIN3D in (B). tRNA is shown as a gray stick model.

ures 5B and C, and 6A) (22). However, the α0 helix is not formed in the structure of hMePCE complexed with only SAH (PDB ID: 5UNA), and this is also the case with the structure of hBCDIN3D complexed with SAH (Figures 1A and 5B, right). Thus, the conserved N-terminal region of hBCDIN3D with aromatic rings (Y37 and F40) could also form an α-helix in the presence of the substrate tRNA^{His} and recognize the 5′-phosphate of tRNA^{His} and the 3′-single-stranded region of tRNA^{His} (Figure 5C). Y37 could recognize the 5′-phosphate of tRNA^{His} during the methylation reaction and Phe40 could stack with the 5′-G_{-1} nucleoside of tRNA^{His}. In support of this proposal, the Y37F, Y37A and F40A mutants reduced the methylation activity with the tRNA^{His} transcript to extents of <10% of that of wild-type hBCDIN3D at the reaction end point (Figure 5D).

In the structure of hMePCE complexed with SAH and 7SK SL1p, the α7 helix between β6 and β7 interacts with the 5′-region of SL1p (Figures 2A and 5E). This interaction relocates the γ-phosphate of 5′-G_1 of SL1p to the catalytic position, together with α0 (Figure 5E). On the other hand, the corresponding region between β6 and β7 in hBCDIN3D is five amino acids shorter and forms a short turn, rather than an α-helix (Figures 2A and 5F). The presence of the shorter loop between β6 and β7 of hBCDIN3D and the N-terminal α0 helix could allow the 5′-end G_{-1}, which is unpaired with A_{73} of tRNA^{His}, to deeply penetrate the catalytic site. The α-phosphate of G_{-1} can then reach the catalytic site and become methylated efficiently. The α0 helix could wedge the G_{-1}:A_{73} mispair at the top of the acceptor stem of tRNA^{His} (Figure 5G).

DISCUSSION

In this study, we determined the crystal structure of hBCDIN3D complexed with SAH (Figure 1). Recently, we showed that hBCDIN3D catalyzes the monomethylation of the 5′-monophosphate of cytoplasmic tRNA^{His} *in vitro* and *in vivo*, and that BCDIN3D recognizes the structural features of tRNA^{His} (15,16). It recognizes not only the G_{-1}:A_{73} mispair at the top of the eight-nucleotide-long acceptor helix, but also the G_{-1} itself of tRNA^{His}. Except for tRNA^{His}, there is no other tRNA species with these unique structural features (29). Thus, we concluded that BCDIN3D

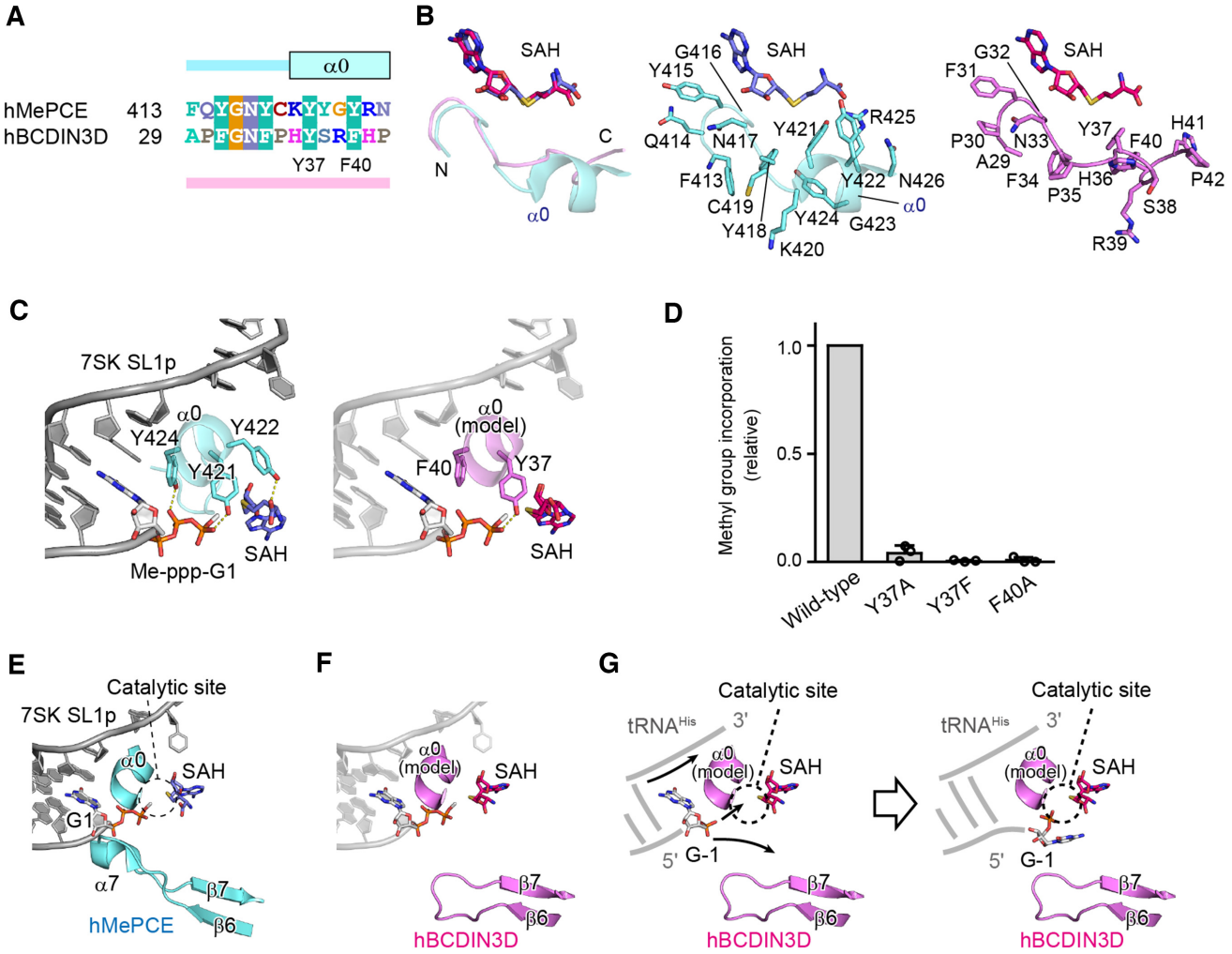

Figure 5. Recognition of the top part of the $tRNA^{His}$ acceptor helix by BCDIN3D. (**A**) Sequence alignment of the N-terminal extended regions of the MTD of hMePCE and hBCDIN3D. In the structure of hMePCE complexed with SL1p, the N-terminal region forms an α-helix (α0). (**B**) Superimposition of the N-terminal region of hBCDIN3D (purple) complexed with SAH onto that of hMePCE (cyan) complexed with SL1p and SAH. The N-terminal region of BCDIN3D does not form an α-helix in the absence of RNA. Detailed views of the N-terminal regions of hMePCE (middle, cyan) and hBCDIN3D (right, purple). (**C**) Interactions between α0 and 7SK SL1p with the Me-ppp cap and SAH (left). The modeled α0 of BCDIN3D (purple) in the structure of hMePCE complexed with SL1p with the Me-ppp cap and SAH (right). Y37 in hBCDIN3D corresponds to Y421 and would interact with the phosphate group. (**D**) The activities of hBCDIN3D variants relative to the wild type (taken as 1.0) under the standard conditions. The reaction mixtures were incubated at 37°C for 1 h. Data are presented as mean ± SD of three independent assays. (**E**) Interactions of α7 between β6 and β7 of hMePCE and the 5′-end of 7SK SL1p with the Me-ppp cap and SAH. (**F**) The modeled α0 and the shorter loop between β6 and β7 of BCDIN3D with the SL1p, in the structure of hMePCE complexed with SL1p. The region between β6 and β7 of hBCDIN3D is shorter than the corresponding region of hMePCE, which forms α7 and interacts with the 5′-end of SL1p. (**G**) A possible mechanism of the α-phosphate methylation of $tRNA^{His}$ by hBCDIN3D. Since an α-helix corresponding to α7 in hMePCE is absent in BCDIN3D, the 5′-monophosphate of G_{-1} of $tRNA^{His}$ is deep within the catalytic pocket for 5′-phosphate methylation. α0 would wedge the G_{-1}:A_{73} mispair at the top of the acceptor helix of $tRNA^{His}$.

is a $tRNA^{His}$-specific 5′-phosphate monomethyltransferase (15,16).

Quite recently, the crystal structure of the MTD of the closely related methyltransferase, a methylphosphate capping enzyme (hMePCE) complexed with SAH and an RNA bearing a 5′-Me-ppp cap, was reported (22). MePCE catalyzes the monomethylation of the 5′-γ-phosphate of 7SK RNA. The amino acid sequence of the MTD of hMePCE and its structure are homologous to those of hBCDIN3D (Figure 2A and B). The comparison of the hBCDIN3D and hMePCE structures has now highlighted the mechanism underlying the different activities between these closely related enzymes (Figures 5 and 6).

In hMePCE, the α7 helix between β6 and β7 interacts with the 5′-end G_1, which base-pairs with C_{108}, and together with the N-terminal α0 helix, the phosphate group of the γ-position is positioned in the catalytic site for the methyl transfer reaction (Figure 6A). On the other hand, in hBCDIN3D, the region corresponding to α7 in hMePCE has fewer amino acids and forms a short loop. Furthermore, $tRNA^{His}$ has a G_{-1}:A_{73} mispair at the top of the acceptor helix. The N-terminal α0 helix wedges the G_{-1}:A_{73}

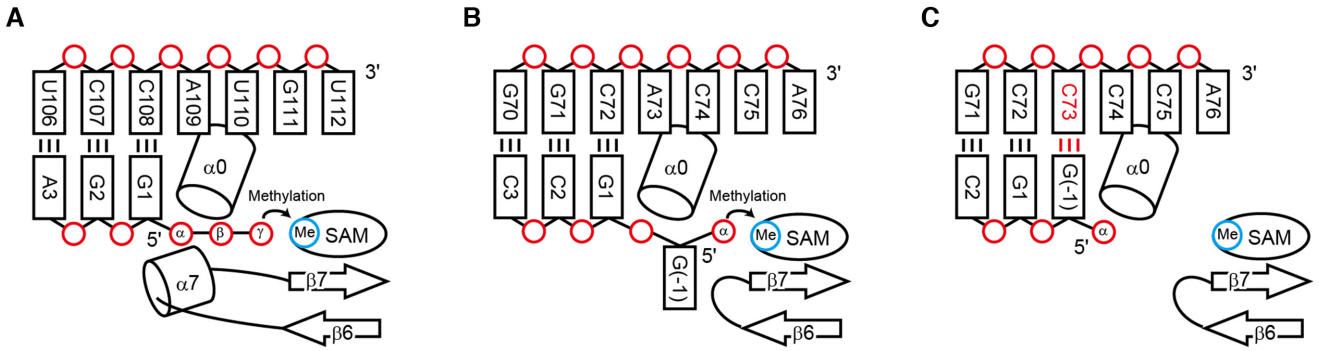

Figure 6. Mechanism of the different activities between MePCE and BCDIN3D. (**A**) 5′-γ-Phosphate methylation of 7SK RNA by MePCE. (**B**) 5′-α-Phosphate methylation of G_{-1} of $tRNA^{His}$ by BCDIN3D. α0 wedges the G_{-1}:A_{73} mispair and the 5′-α-phosphate reaches the catalytic site for methylation. (**C**) $tRNA^{His}$ with G_{-1}:C_{73} is not methylated, since α0 would not wedge the base pair, and the 5′-α-phosphate cannot reach the active site for methylation.

mispair, and the 5′-α-phosphate of the G_{-1} of $tRNA^{His}$ can access the active site for the methyl transfer reaction (Figure 6B). This can explain the previous biochemical data showing that hBCDIN3D exclusively recognizes the G_{-1}:A_{73} mispair at the top of the acceptor helix of $tRNA^{His}$. The $tRNA^{His}$ mutant with the G_{-1}:C_{73} pair cannot be methylated by hBCDIN3D (15). Since the α0 helix cannot wedge the G_{-1}:C_{73} pair at the top of the acceptor helix, the α-phosphate of G_{-1} of $tRNA^{His}$ would not be able to access the active site and thus cannot be methylated (Figure 6C). This mechanism is similar to that observed in the formylation of bacterial methionyl-$tRNA_f^{Met}$ by methionyl-$tRNA_f^{Met}$ formyltransferase (30). The specific loop wedges the C_1:A_{72} mispair at the top of the acceptor helix, characteristic of the initiator tRNA, and the 3′-end of tRNA bends inside the active site.

hBCDIN3D cannot methylate a $tRNA^{His}$ mutant with a 5′-triphosphate group at its 5′-end *in vitro* (Supplementary Figure S2C). The 5′-triphosphate group could not enter the catalytic pocket, since there is not enough space to accommodate the triphosphate in the pocket when $tRNA^{His}$ with a 5′-triphosphate binds to hBCDIN3D in the same manner as $tRNA^{His}$ with a 5′-monophosphate.

The recognition mechanism of the guanine base of G_{-1} of $tRNA^{His}$ by hBCDIN3D is still unclear. The loop between β6 and β7 might specifically recognize the guanine base of G_{-1}. Clarification of the detailed mechanism of the monomethylation of the 5′-monophosphate of $tRNA^{His}$ awaits the determination of the structure of BCDIN3D complexed with $tRNA^{His}$.

The biological role of the 5′-monomethylation of cytoplasmic $tRNA^{His}$ remains enigmatic. It does not significantly affect the steady-state level of $tRNA^{His}$ in human cells and fly ovary, and it does not change the aminoacylation efficiency or level by histidyl-tRNA synthetase (12,15). As discussed (15), the 5′-monomethylation of $tRNA^{His}$ might be involved in $tRNA^{His}$ fragments' generation or their stability under stress conditions and participate in various cellular functions beyond their established roles in protein synthesis. BCDIN3D is overexpressed in human breast cancer, and this overexpression is associated with cellular invasion and poor prognosis in triple-negative breast cancer (10,11). Although the molecular basis of the involvement of BCDIN3D in the tumorigenic phenotype of breast cancer has remained elusive, the structure of hBCDIN3D presented in this study will provide useful information for the design of anticancer drugs.

DATA AVAILABILITY

Coordinates and structure factors for the crystal structure of hBCDIN3D complexed with SAH have been deposited in the Protein Data Bank, under the accession code 6L8U.

SUPPLEMENTARY DATA

Supplementary Data are available at NAR Online.

ACKNOWLEDGEMENTS

We thank Yuka Fujimoto for technical assistance. We also thank the beamline staff of BL-17A (KEK, Tsukuba) for technical assistance during data collection.

FUNDING

JSPS [LS135 (in part) to K.T., 18H03980 to K.T.]; Ministry of Education, Culture, Sports, Science and Technology [26113002 to K.T.]; Takeda Science Foundation; Uehara Memorial Foundation; Terumo Foundation for Life Sciences and Arts; Princess Takamatsu Cancer Research Fund. Funding for open access charge: JSPS [18H03980 to K.T.].
Conflict of interest statement. None declared.

REFERENCES

1. Xhemalce,B., Robson,S.C. and Kouzarides,T. (2012) Human RNA methyltransferase BCDIN3D regulates microRNA processing. *Cell*, **151**, 278–288.
2. Zhu,W. and Hanes,S.D. (2000) Identification of *Drosophila* bicoid-interacting proteins using a custom two-hybrid selection. *Gene*, **245**, 329–339.
3. Shumyatsky,G.P., Tillib,S.V. and Kramerov,D.A. (1990) B2 RNA and 7SK RNA, RNA polymerase III transcripts, have a cap-like structure at their 5′ end. *Nucleic Acids Res.*, **18**, 6347–6351.
4. Gupta,S., Busch,R.K., Singh,R. and Reddy,R. (1990) Characterization of U6 small nuclear RNA cap-specific antibodies. Identification of gamma-monomethyl-GTP cap structure in 7SK and several other human small RNAs. *J. Biol. Chem.*, **265**, 19137–19142.

5. Jeronimo,C., Forget,D., Bouchard,A., Li,Q., Chua,G., Poitras,C., Therien,C., Bergeron,D., Bourassa,S., Greenblatt,J. *et al.* (2007) Systematic analysis of the protein interaction network for the human transcription machinery reveals the identity of the 7SK capping enzyme. *Mol. Cell*, **27**, 262–274.
6. Shuman,S. (2007) Transcriptional networking cap-tures the 7SK RNA 5′-γ-methyltransferase. *Mol. Cell*, **27**, 517–519.
7. Diribarne,G. and Bensaude,O. (2009) 7SK RNA, a non-coding RNA regulating P-TEFb, a general transcription factor. *RNA Biol.*, **6**, 122–128.
8. Peterlin,B.M., Brogie,J.E. and Price,D.H. (2012) 7SK snRNA: a noncoding RNA that plays a major role in regulating eukaryotic transcription. *Wiley Interdiscip. Rev. RNA*, **3**, 92–103.
9. Cosgrove,M.S., Ding,Y., Rennie,W.A., Lane,M.J. and Hanes,S.D. (2012) The Bin3 RNA methyltransferase targets 7SK RNA to control transcription and translation. *Wiley Interdiscip. Rev. RNA*, **3**, 633–647.
10. Liu,R., Wang,X., Chen,G.Y., Dalerba,P., Gurney,A., Hoey,T., Sherlock,G., Lewicki,J., Shedden,K. and Clarke,M.F. (2007) The prognostic role of a gene signature from tumorigenic breast-cancer cells. *N. Engl. J. Med.*, **356**, 217–226.
11. Yao,L., Chi,Y., Hu,X., Li,S., Qiao,F., Wu,J. and Shao,Z.M. (2016) Elevated expression of RNA methyltransferase BCDIN3D predicts poor prognosis in breast cancer. *Oncotarget*, **7**, 53895–53902.
12. Zhu,L., Liao,S.E., Ai,Y. and Fukunaga,R. (2019) RNA methyltransferase BCDIN3D is crucial for female fertility and miRNA and mRNA profiles in *Drosophila* ovaries. *PLoS One*, **14**, e0217603.
13. Suzuki,T., Ikeuchi,Y., Noma,A., Suzuki,T. and Sakaguchi,Y. (2007) Mass spectrometric identification and characterization of RNA-modifying enzymes. *Methods Enzymol.*, **425**, 211–229.
14. Rosa,M.D., Hendrick,J.P., Jr., Lerner,M.R., Steitz,J.A. and Reichlin,M. (1983) A mammalian $tRNA^{His}$-containing antigen is recognized by the polymyositis-specific antibody anti-Jo-1. *Nucleic Acids Res.*, **11**, 853–870.
15. Martinez,A., Yamashita,S., Nagaike,T., Sakaguchi,Y., Suzuki,T. and Tomita,K. (2017) Human BCDIN3D monomethylates cytoplasmic histidine transfer RNA. *Nucleic Acids Res.*, **45**, 5423–5436.
16. Tomita,K. and Liu,Y. (2018) Human BCDIN3D is a cytoplasmic tRNA(His)-specific 5′-monophosphate methyltransferase. *Front. Genet.*, **9**, 305.
17. Kabsch,W. (2010) XDS. *Acta Crystallogr. D: Biol. Crystallogr.*, **66**, 125–132.
18. McCoy,A.J., Grosse-Kunstleve,R.W., Adams,P.D., Winn,M.D., Storoni,L.C. and Read,R.J. (2007) Phaser crystallographic software. *J. Appl. Crystallogr.*, **40**, 658–674.
19. Waterhouse,A., Bertoni,M., Bienert,S., Studer,G., Tauriello,G., Gumienny,R., Heer,F.T., de Beer,T.A.P., Rempfer,C., Bordoli,L. *et al.* (2018) SWISS-MODEL: homology modelling of protein structures and complexes. *Nucleic Acids Res.*, **46**, W296–W303.
20. Afonine,P.V., Grosse-Kunstleve,R.W., Echols,N., Headd,J.J., Moriarty,N.W., Mustyakimov,M., Terwilliger,T.C., Urzhumtsev,A., Zwart,P.H. and Adams,P.D. (2012) Towards automated crystallographic structure refinement with phenix.refine. *Acta Crystallogr. D: Biol. Crystallogr.*, **68**, 352–367.
21. Emsley,P., Lohkamp,B., Scott,W.G. and Cowtan,K. (2010) Features and development of Coot. *Acta Crystallogr. D: Biol. Crystallogr.*, **66**, 486–501.
22. Yang,Y., Eichhorn,C.D., Wang,Y., Cascio,D. and Feigon,J. (2019) Structural basis of 7SK RNA 5′-gamma-phosphate methylation and retention by MePCE. *Nat. Chem. Biol.*, **15**, 132–140.
23. Doxtader,K.A., Wang,P., Scarborough,A.M., Seo,D., Conrad,N.K. and Nam,Y. (2018) Structural basis for regulation of METTL16, an *S*-adenosylmethionine homeostasis factor. *Mol. Cell*, **71**, 1001.e1004.
24. Ruszkowska,A., Ruszkowski,M., Dauter,Z. and Brown,J.A. (2018) Structural insights into the RNA methyltransferase domain of METTL16. *Sci. Rep.*, **8**, 5311.
25. Liu,R.J., Long,T., Li,J., Li,H. and Wang,E.D. (2017) Structural basis for substrate binding and catalytic mechanism of a human RNA:m5C methyltransferase NSun6. *Nucleic Acids Res.*, **45**, 6684–6697.
26. Finer-Moore,J., Czudnochowski,N., O'Connell,J.D., 3rd, Wang,A.L. and Stroud,R.M. (2015) Crystal structure of the human tRNA m(1)A58 methyltransferase-tRNA(3)(Lys) complex: refolding of substrate tRNA allows access to the methylation target. *J. Mol. Biol.*, **427**, 3862–3876.
27. Song,J., Teplova,M., Ishibe-Murakami,S. and Patel,D.J. (2012) Structure-based mechanistic insights into DNMT1-mediated maintenance DNA methylation. *Science*, **335**, 709–712.
28. Holm,L. and Rosenström,P. (2010) Dali server: conservation mapping in 3D. *Nucleic Acids Res.*, **38**, W545–W549.
29. Juhling,F., Morl,M., Hartmann,R.K., Sprinzl,M., Stadler,P.F. and Putz,J. (2009) tRNAdb 2009: compilation of tRNA sequences and tRNA genes. *Nucleic Acids Res.*, **37**, D159–D162.
30. Schmitt,E., Panvert,M., Blanquet,S. and Mechulam,Y. (1998) Crystal structure of methionyl-tRNAfMet transformylase complexed with the initiator formyl-methionyl-tRNAfMet. *EMBO J.*, **17**, 6819–6826.